Structural and Dynamic Properties of the HIV-1 Tat Transduction Domain in the Free and Heparin-Bound States†

Susanna Hakansson and Michael Caffrey*

Department of Biochemistry and Molecular Biology, University of Illinois at Chicago, Chicago, Illinois 60612

Received December 30, 2002

ABSTRACT: An 11-residue basic domain of the HIV-1 tat protein, termed the tat transduction domain (TTD), has been shown to mediate transfer of biomolecules across biological membranes. The mechanism of TTD-mediated membrane translocation is currently unknown but thought to involve binding to heparan sulfate, which is found in proteoglycans that are ubiquitously present on cell surfaces. To study the mechanism of TTD-mediated membrane translocation, the TTD was fused to the C-terminus of a model cargo protein, the IgG binding domain of streptococcal protein G (PG) to form PG-TTD. NMR studies of PG-TTD in the free state indicated that the structure of the PG moiety of PG-TTD was not perturbed by the presence of the TTD and that the TTD moiety is in an extended conformation. Heteronuclear relaxation measurements of PG-TTD in the free state show that the TTD moiety of PG-TTD is relatively mobile (e.g., the average S^2 value of the TTD and PG core are ∼0.54 and ∼0.84, respectively). PG-TTD has been shown to bind to heparin by isothermal titration calorimetry ($K_D = 0.37$ μM, $\Delta H = -12$ kcal/mol, $\Delta S = -11$ cal/mol/T). NMR spectroscopy demonstrated that heparin binds to the TTD moiety of PG-TTD. The heteronuclear relaxation measurements of PG-TTD in complex with heparin show that the TTD becomes less dynamic when bound to heparin (average S^2 value of the TTD is 0.69 in the presence of heparin). A model for the first step of TTD-mediated entry into cells is presented.

An 11-residue basic region of HIV-1 tat (amino acid sequence = YGRKKRRQRRR), termed the tat transduction domain (TTD),[1] has been shown to mediate transfer of HIV-1 tat across biological membranes (*1*, *2*). The transduction abilities of HIV-1 tat are thought to play numerous roles in the progression and pathogenesis of AIDS (*3*−*5*). Interestingly, proteins containing the TTD translocate across biological membranes in cell culture and in living animals. For example, Schwarze et al. (*6*) have shown that β-galactosidase containing the 11 residues of the TTD at the amino terminus can be delivered by intraperitoneal injection to virtually all tissues in mice. In addition, it has been established that the TTD can be used for intracellular delivery of DNA and drug-like compounds as well as proteins (reviewed in ref *7*). As a consequence, TTD fusions can be envisioned as delivery tools for a wide variety of diagnostic and therapeutic agents to diverse cell types.

Despite the importance of the TTD in AIDS pathogenesis and the increasing use of the TTD in biochemical and medical studies, little is known about the mechanism of TTD-mediated membrane translocation. In the simplest model, the TTD must exist in two states: (i) a free solution state, which corresponds to the extracellular and intracellular conformation; (ii) a membrane-bound state (or states), in which TTD is bound to protein, carbohydrate, and/or lipids. As a consequence, a detailed understanding of the TTD mechanism requires knowledge of the structural and dynamic properties of the TTD solution and membrane-bound states. Recently, heparan sulfate, which is found in proteoglycans ubiquitously present on the cell surface, has been implicated in TTD-mediated internalization. For example, it has been shown that the HIV-1 tat protein, which naturally contains the TTD at residues 47−57, binds to soluble heparin, an analogue of heparan sulfate, via the basic residues within TTD (*8*, *9*). Moreover, mutant cell lines lacking heparan sulfate have been shown to be deficient in tat-mediated membrane translocation (*10*). However, a different mechanism, which does not require heparan sulfate, has been suggested for TTD-mediated entry of cargo proteins (*11*). Interestingly, Richard et al. have recently shown evidence that TTD-mediated entry, as well as those of other basic peptides, occurs by endocytosis (*12*, *13*). In the present work, the TTD has been fused to the C-terminus of a model cargo protein, the IgG-binding domain of streptococcal protein G (PG). The structural and dynamic properties of the free and heparin bound states of the TTD have been characterized by NMR spectroscopy to lend insight into the mechanism of TTD-mediated membrane translocation.

EXPERIMENTAL PROCEDURES

Preparation of PG-TTD. The preparation of PG-TTD is described elsewhere (*14*). The resulting PG-TTD construct consists of 77 residues: (a) the 56 residues of PG (*15*), (b) a six-residue linker region (amino acid sequence =

† This work was supported by startup funds from the University of Illinois at Chicago.

* To whom correspondence should be addressed.

[1] Abbreviations: FGF, fibroblast growth factor; FITC, fluorescein isothiocyanate; GFP, green fluorescent protein; GST, glutathione *S*-transferase; HIV, human immunodeficiency virus; ITC, isothermal titration calorimetry; PG, IgG binding domain of streptococcal protein G; PG-TTD, TTD fused to C-terminus of PG; TTD, HIV-1 tat transduction domain.

10.1021/bi020715+ CCC: $25.00
Published on Web 07/01/2003

PGGPAS), (c) TTD (amino acid sequence = YGRKKRRQRRR), (d) a four-residue cloning artifact at the C-terminus (amino acid sequence = GGGG). The expression and purification of PG-TTD has been previously described (*14*). The identity of PG-TTD was confirmed by mass spectrometry.

NMR Assignments and Dynamic Studies. For the NMR experiments, ^{15}N-labeled and ^{13}C/^{15}N-labeled PG-TTD were prepared by growing the appropriate *Escherichia coli* BL21-(DE3) strain in minimal media supplemented with $^{15}NH_4Cl$ (Martek Biosciences, Columbia, Maryland) and ^{13}C-glucose (Isotec, Miamisburg, Ohio) as previously described (*16*). NMR experiments of PG-TTD in the free state contained 1 mM PG-TTD in 100 mM PO_4 /pH 6.0, 10% D_2O. NMR experiments of PG-TTD/heparin contained 1 mM PG-TTD, 1 mM heparin in 100 mM PO_4 /pH 6.0, 10% D_2O. Heparin (lyophylized pig intestine heparin, average molecular weight = 6000, Sigma, St. Louis) concentrations were determined by the uronic acid assay (*17*). All NMR experiments were preformed with a Bruker DRX600 spectrometer equipped with a triple resonance probe at 27 °C. For the NMR assignment of the backbone resonances, the experiments included ^{15}N-edited HSQC, 3D ^{15}N-edited TOCSY (mixing time = 70 ms), 3D ^{15}N-edited NOESY (mixing time = 150 ms), HNCA, HNCOCA, and HNCO. The ^{15}N R_z (1/ T_1), R_{xy} (1/ T_2) and HNOE values were measured by standard pulse sequences (reviewed in ref *18*). In the case of free PG-TTD, a total of seven data sets were collected to measure R_z with delay values of 11.8, 31.8, 61.8, 121.8, 241.8, 481.8, and 721.8 ms; a total of seven data sets were collected to measure R_{xy} with delay values of 8, 16, 32, 64, 128, 192, and 256 ms. In the case of PG-TTD/heparin, a total of six data sets were collected to measure R_z with delay values of 11.8, 51.8, 101.8, 201.8, 401.8, and 801.8 ms; a total of six data sets were collected to measure R_{xy} with delay values of 8, 40, 80, 120, 160, and 200 ms. All NMR data were processed with NMRPipe (*19*). The decays of cross-peak intensities with time in the $^{15}N-R_z$ and R_{xy} experiments were fit to a single exponential by a nonlinear least-squares fit with fitting errors typically less than 5% (Kaleidagraph 3.08, Synergy Software, Reading, Pennsylvania). HNOE values for each given residue were calculated as the intensity ratio (I/I_0) of the ^{15}N-^{1}H correlation peak in the presence (I) and absence (I_0) of proton saturation during the relaxation delay of 5 s. Errors in the HNOE were estimated to be ± 0.10. Analysis of rotational diffusion and internal mobility was performed by the program Tensor version 2.0 (*20*). On the basis of the PG structure (*21*), R_{xy}/R_z ratios of residues 3−56 (the core structure of PG) and a Monte Carlo error analysis, the appropriate diffusion model was determined to be isotropic in the case of free PG-TTD and fully anisotropic in the case of PG-TTD bound to heparin. The appropriate model for rotational diffusion was then used in a Lipari-Szabo type analysis of the internal mobility (*22*). Due to spectral overlap residues 2, 68, and 70 are missing from the analysis PG-TTD in the free state and residues 2, 61, 65, 66, 69, 70, 71, and 73 are missing from the analysis of PG-TTD in the complex with heparin. Molecular dynamics simulations were performed using CNS (*23*). The program MOLMOL was used for molecular graphics (*24*).

Heparin Titrations. Isothermal titatration calorimetry (ITC) was performed on a MicroCal VP−ITC. Solutions were degassed under vacuum prior to use. The heat off dilution, which was subtracted from the titration, was determined by injecting heparin into buffer. Experimental conditions were 7.8 μM PG-TTD, 100 mM PO_4/pH 6.0 at 25 °C. Titrations were performed by injecting 5 μL of a 142 μM heparin solution in 100 mM PO_4/pH 6.0. Thermodynamic data were derived from the Origin software provided by the manufacturer. For the NMR titrations, aliquots of the heparin stock solution were added to a NMR tube containing 317 μM PG-TTD in 100 mM PO_4/pH 6.0 at 27 °C. CD spectra were recorded on a Jasco J-710 spectropolarimeter with a 0.1-cm path length at 23 °C.

RESULTS

Structural Properties of PG-TTD in the Free State. For the study of the TTD, we have chosen to fuse it to the C-terminus of PG, which is well expressed in *E. coli* and has been extensively characterized by NMR spectroscopy (*15*, *21*, *25*). For NMR studies of protein structure and dynamics, the first step is the assignment of the chemical shifts. The ^{1}H, ^{13}C, and ^{15}N of the PG-TTD backbone were assigned using standard heteronuclear NMR experiments (cf. Experimental Procedures). As shown by Figure 1a, the ^{15}N-edited HSQC spectrum of PG-TTD is well dispersed and very similar to that of PG (*21*, *25*). There are 19 new correlations observed in the spectrum of PG-TTD. This number is consistent with the introduction of 11 TTD amino acids and eight additional amino acids in the PG-TTD construct (there are also two added prolines, which do not exhibit correlations in the ^{15}N-edited HSQC experiment). Interestingly, the backbone chemical shifts of the TTD residues (and those of the other added residues) are close to the random coil values, suggesting that the TTD tail is relatively unstructured in aqueous solution (Figure 1b). Moreover, the TTD residues do not exhibit NOE patterns in the ^{15}N-edited NOESY spectrum that would indicate regular secondary structure or tertiary structure. These observations are in agreement with CD and NMR studies of the TTD peptide in the absence of PG (Caffrey, unpublished data). A number of PG residues exhibit small perturbations of their backbone chemical shifts with respect to PG in the absence of the TTD, suggesting that the presence of the TTD sequence perturbs their local environment. However, on the basis of the observation that the majority of the PG residues only exhibit small chemical shift perturbations, the structure of PG can be inferred to be that of the wild-type PG. As shown by Figure 1c, the structural perturbations are clearly limited to those residues in close contact with the added TTD sequence, which follows PG residue 56. Thus, the added sequence does not perturb the PG structure and does not interact significantly with the PG core.

Dynamic Properties of PG-TTD in the Free State. The dynamic properties of PG-TTD were characterized by determination of heteronuclear relaxation rates, which have been widely used to investigate the backbone dynamics of proteins (*27*, *28*). The $^{15}N-R_z$ and R_{xy} relaxation rates and the ^{1}H-^{15}N NOE (HNOE) were determined for each residue in PG-TTD (Figure 2a). In general, R_z, R_{xy}, and HNOE of the PG moiety of PG-TTD are very similar to those previously observed for the wild-type PG (*25*). Interestingly, the TTD sequence exhibits lower values of R_z, R_{xy} and the HNOE than the PG. For example, the average R_z, R_{xy} and

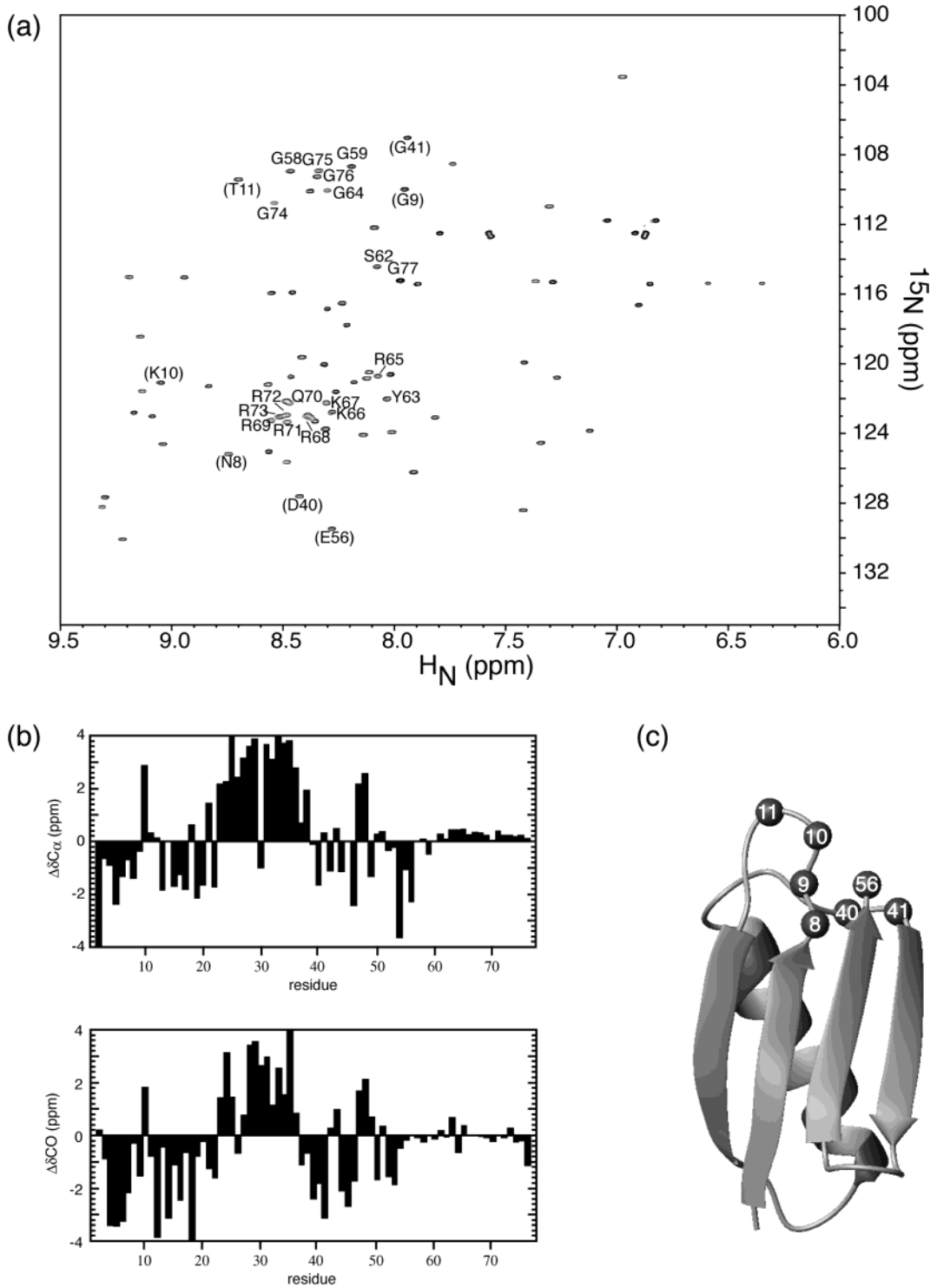

FIGURE 1: Structural properties of PG-TTD in the free state. (a) ^{15}N-edited HSQC spectrum of PG-TTD. The TTD residues (and the residues that link TTD to PG) are labeled. PG residues that exhibit H_N that are perturbed by >0.2 ppm are labeled with parentheses. Experimental conditions were 300 μM protein in 100 mM PO_4/pH 6.0, 10% D_2O at 27 °C. (b) Backbone chemical shifts of PG-TTD with respect to random coil values. Random coil values were taken from Wishart and Case (*26*). (c) Location of PG residues perturbed by the addition of a C-terminal TTD sequence. The structure of PG is that of Gronenborn et al. (*21*).

the HNOE values of the PG (residues 1−56) are 1.99 s^{-1}, 6.62 s^{-1}, and 0.70, respectively; the average R_z, R_{xy} and the HNOE values of the TTD (residues 63−73) are 1.60 s^{-1}, 4.36 s^{-1}, and 0.15, respectively. This difference suggests that, at least at a qualitative level, the TTD moiety is more mobile than the PG core. To better interpret the dynamic properties of PG-TTD, the three relaxation parameters were analyzed by the program Tensor (*20*), which determines the appropriate rotational diffusion model and fits the data to a Model-free analysis of internal mobility. On the basis of the R_{xy}/R_z ratios of the PG core residues, the isotropic model was deemed most appropriate. The resulting overall correlation time is estimated to be 4.74 ± 0.05 ns. Many of the residues fit to the simplest model of internal mobility, which requires one variable S^2. Residues 13 and 75−77 require an R_{ex} term to include conformational exchange on the microsecond to

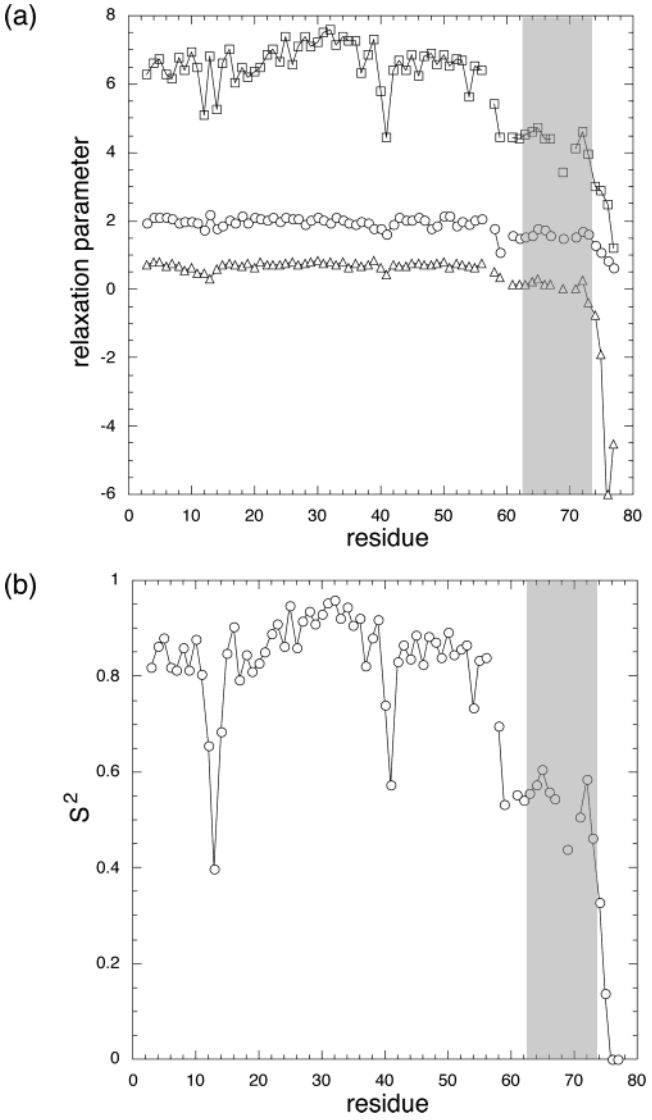

FIGURE 2: Dynamic properties of PG-TTD. (a) R_z (circles) R_{xy} (squares) HNOE (triangles); (b) Order parameters (S^2) of PG-TTD based on a isotropic model of rotational diffusion. TTD (residues 63−73) are denoted by a shaded box. Experimental conditions were 1 mM PG-TTD in 100 mM PO_4/pH 6 at 27 °C at 600 MHz.

millisecond time scale. Residues 6, 8−14, 18, 20, 35, 40, 41, 43, 51, 54, 55, 58, 59, 61−67, 69, 71−77 (which largely includes TTD residues 63−73) require an effective internal correlation time τ_e to fit the relaxation parameters. No residues require the extended model free formalism (*25*). The resulting S^2 values are shown in Figure 2b. As expected from the R_z, R_{xy}, and HNOE values for the PG core, the derived S^2 values are again very similar to the wild-type PG (*25*), suggesting that the dynamic properties of PG are not perturbed by the presence of the TTD sequence. Interestingly, the average S^2 value of TTD is 0.54 and the average S^2 value for PG is 0.84, consistent with the notion that in the free state the PG core is relatively rigid and the TTD tail is relatively mobile.

Thermodynamics of Heparin Binding to PG-TTD. As discussed in the Introduction, previous work suggested an important role of heparan sulfate in the translocation of HIV-1 tat (*8*−*10*). To better understand the mechanism of TTD-mediated entry, we have characterized the thermodynamic properties of heparin, a naturally occurring analogue

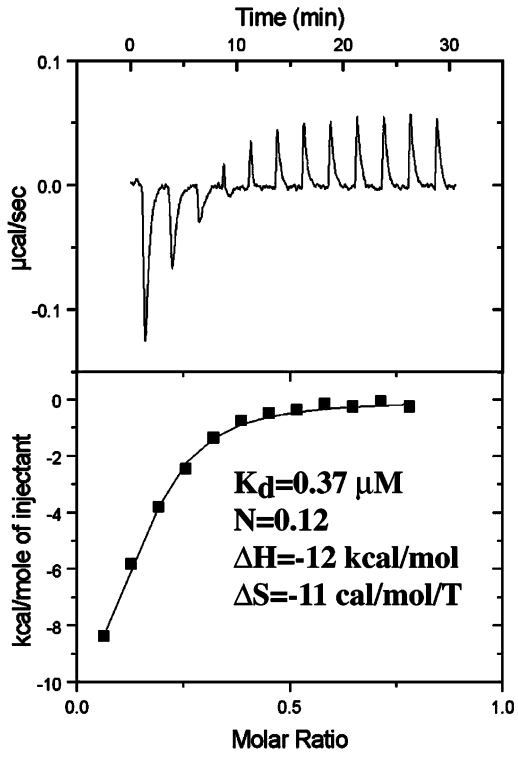

FIGURE 3: Heparin binds to PG-TTD as shown by ITC titration of PG-TTD by heparin. Experimental conditions were 7.8 μM PG-TTD, 100 mM PO_4/pH 6.0 at 25 °C. Titrations were performed by injecting 5 μL of a 142 μM heparin solution in 100 mM PO_4/pH 6.0.

of heparan sulfate (*29*), binding to PG-TTD by ITC. The results of the ITC analysis are shown in Figure 3. First, note that the dissociation constant of 0.37 μM is consistent with the notion of a relatively strong affinity of PG-TTD for heparin. Second, the derived n value of 0.12 suggests that ∼8 PG-TTD molecules bind to 1 heparin molecule, which in the present case possesses an average molecular weight of ∼6000 and thus consists of ∼20 negatively charged monosaccharide units. Third, the derived ΔH of the complex formation is −12 kcal/mol and the derived ΔS is −11 cal/mol/T, suggesting that complex formation is enthalpy driven. The negative enthalpy is consistent with the formation of energetically favorable electrostatic interactions between the positively charged side chains of TTD and the negatively charged sulfate groups of heparin. On the other hand, the negative ΔS suggests that entropy is decreased by formation of the PG-TTD/heparin complex (to be discussed below).

NMR and CD Characterization of Heparin Binding to PG-TTD. To further characterize the PG-TTD/heparin complex, ^{15}N-edited HSQC of ^{15}N-labeled PG-TTD was used as an assay of protein−ligand interactions (*30*). In Figure 4a, the effects of adding soluble heparin to ^{15}N-labeled PG-TTD are shown. First, note that only a subset of the resonances move during the titration. The only resonances that move correspond to the TTD resonances, which indicate that they are in close association with heparin. Examples include Y63, K66, and Q70. The PG-TTD/heparin complex is in fast exchange, as indicated by the presence of only one set of resonances. The exchange rate can be estimated by the maximal chemical shift perturbation. At saturating concentrations of heparin, R69 exhibits the largest change in H_N chemical shift (0.32 ppm), which indicates that the exchange

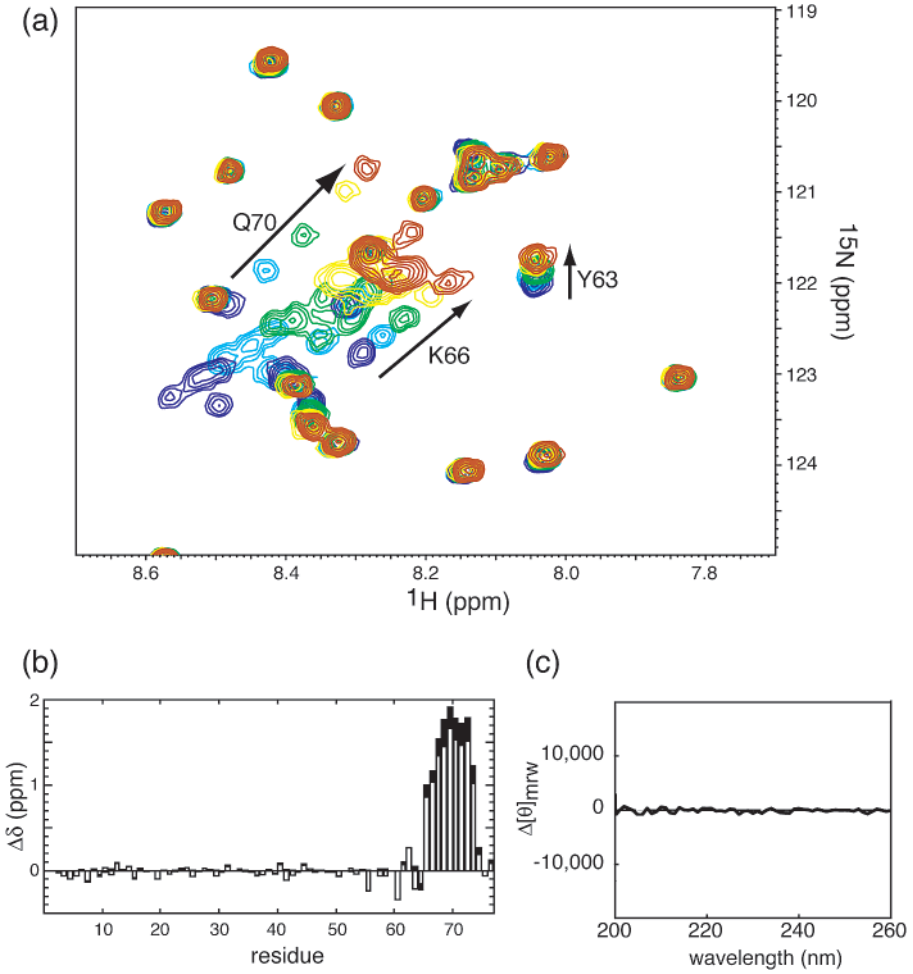

FIGURE 4: Effects of heparin binding on PG-TTD structure. (a) ^{15}N-edited HSQC spectra of PG-TTD in the presence of increasing concentrations of heparin (blue = no heparin, cyan = 22 μM heparin, green = 44 μM heparin, yellow = 65 μM heparin, red = 105 μM heparin). Experimental conditions were 317 μM PG-TTD, 100 mM PO_4/pH 6.0, 5% D_2O at 27 °C. (b) H_N (solid bars) and ^{15}N (open bars) chemical shift perturbations of PG-TTD in the presence of heparin. Experimental conditions were 317 μM PG-TTD, 300 μM heparin in 100 mM PO_4/pH 6.0, 5% D_2O at 27 °C. (c) CD difference spectrum of PG-TTD and PG-TTD/heparin. The PG-TTD spectrum was corrected for buffer. The PG-TTD/heparin spectrum was corrected for heparin/buffer. Experimental conditions were 30 μM PG-TTD, 300 μM heparin in 100 mM PO_4/pH 6.0 at 23 °C.

rate between the bound and free states is greater than 190 Hz or 1200 s^{-1}. The location of heparin binding to PG-TTD can be inferred from a plot of chemical shift perturbation versus residue number (Figure 4b). First note that the PG moiety (residues 1−56) does not exhibit significant chemical shift changes, consistent with the notion that heparin does not bind to PG. In contrast, TTD residues (residues 63−73) are clearly perturbed. We were next interested in the conformation of TTD when bound to heparin. In the absence of heparin, the chemical shift and relaxation properties of PG-TTD indicate that TTD is in a flexible extended conformation (discussed above). In the presence of heparin, the simultaneous upfield shift of the TTD H_N and ^{15}N could be taken to indicate the adoption of helical structure (*26*). On the contrary, the spectral dispersion of the TTD residues does not increase in the presence of heparin (cf., Figure 4a), suggesting a continued absence of regular secondary structure. Moreover, examination of the 3D ^{15}N-edited NOESY spectrum of PG-TTD/heparin complex did not reveal the presence of shortrange (or longrange) NOEs which would be characteristic of a regular secondary (or tertiary) structure in the TTD. To further probe the effects of heparin binding, the secondary structure of the PG-TTD in the presence and absence of heparin was assayed by difference CD spectropolarimetry. As shown by Figure 4c, no change in the PG-TTD CD spectrum is observed in the presence of excess heparin (or at a 1:1 ratio, data not shown). Thus, it can be inferred that heparin does not induce a change in secondary structure of PG-TTD and that TTD remains in an extended conformation.

Dynamic Properties of the PG-TTD/Heparin Complex. As shown above, the dynamic properties of PG-TTD in the free state suggest that TTD is relatively mobile and that this mobility may be functionally important (to be discussed below). Moreover, the thermodynamic studies presented above suggest that the entropy of PG-TTD and/or heparin is decreased upon complex formation. To further characterize the dynamic properties of TTD when complexed to heparin, we performed the standard set of heteronuclear NMR relaxation experiments in the presence of an equimolar concentration of heparin. The R_z, R_{xy}, and HNOE of PG-TTD in the presence of heparin are shown in Figure 5a. First note that average R_z, R_{xy}, and the HNOE values of the PG core (residues 1−56) in the presence of heparin are 1.69 s^{-1}, 9.47 s^{-1}, and 0.68, which are somewhat different than the relaxation parameters of the PG core in the free state. For

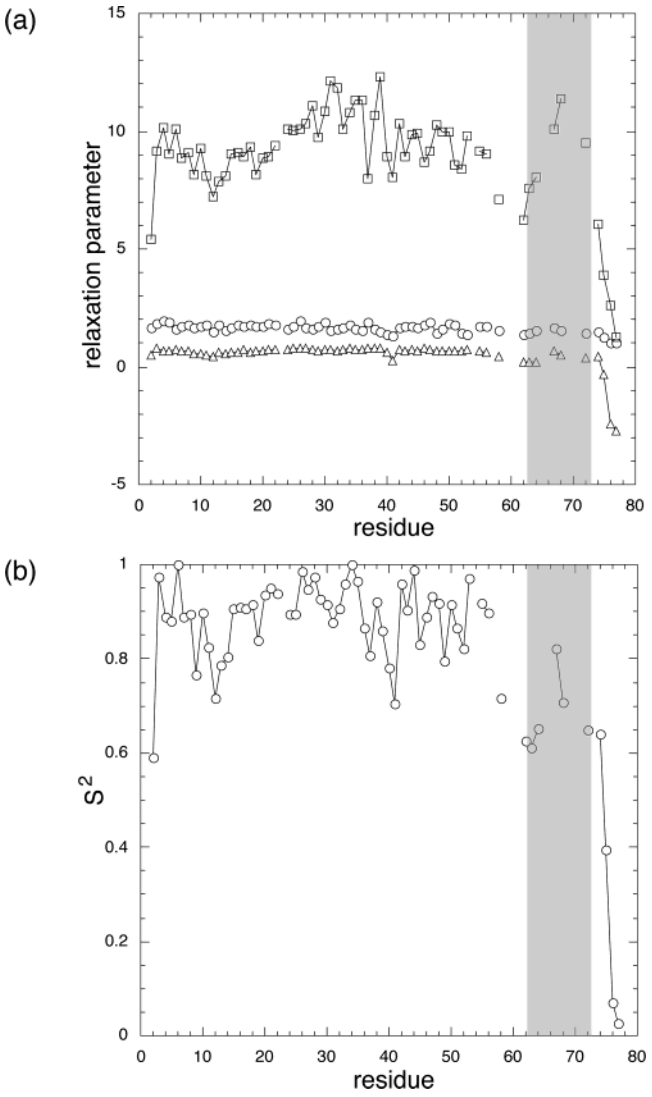

FIGURE 5: Dynamic properties of PG-TTD in the presence of heparin. (a) R_z (circles), R_{xy} (squares), HNOE (triangles); (b) Order parameters (S^2) of PG-TTD based on a fully anisotropic model of rotational diffusion. TTD (residues 63−73) are denoted by a shaded box. Experimental conditions were 1 mM PG-TTD/heparin in 100 mM PO_4/pH 6 at 27 °C at 600 MHz.

example, the average R_{xy} rate of the PG core is 6.62 s^{-1} in the free state and 9.47 s^{-1} in the presence of heparin, which is consistent with the larger molecular weight of the PG-TTD/heparin complex (∼9 kDa versus ∼15 kDa). Interestingly, the changes in the relaxation parameters, with respect to their corresponding free state values shown in Figure 2a, clearly indicate that the TTD tail is less mobile in the presence of heparin. For example, the average R_z, R_{xy}, and the HNOE values of the TTD bound to heparin are 1.51 s^{-1}, 8.81 s^{-1}, and 0.36, respectively; the average R_z, R_{xy} and the HNOE values of the TTD in the free state are 1.60 s^{-1}, 4.36 s^{-1}, and 0.15, respectively. It is important to note that the ITC results suggest that multiple PG-TTD bind to 1 heparin molecule and thus the NMR experiments are actually observing a mixture of PG-TTD/heparin complexes in fast exchange. Nonetheless, the relaxation parameters can be interpreted on a qualitative basis. On the basis of the R_{xy}/R_z ratios of the PG core, the fully anisotropic model was deemed to be most appropriate. The resulting diffusion tensor parameters are $D_{xx} = 1.95 \times 10^{-7}$ s^{-1}, $D_{yy} = 2.29 \times 10^{-7}$ s^{-1}, and $D_{zz} = 3.36 \times 10^{-7}$ s^{-1}. In contrast to the PG-TTD free state, fewer residues fit to the simplest model requiring only S^2. Residues 31 and 39 require a R_{ex} term. Residues 2, 5, 7−16, 18−20, 29, 33, 35, 40−43, 48, 51, 52, 55, 56, 58, 62, 74, 75, and 77 require an effective internal correlation time τ_e to fit the relaxation parameters. Residues 4, 30, 32, 36, 45, 49, 50, 63, 64, 67, 68, 72, and 76, which include all of the observed TTD residues, require R_{ex} and τ_e terms to fit the relaxation parameters. No residues require the extended model free formalism. As shown in Figure 5b, the S^2 of PG are essentially unchanged with respect to PG-TTD in the free state (average $S^2 = 0.89$). Interestingly, the S^2 values of TTD are notably increased with the largest change occurring at residue 67 ($\Delta S^2 = 0.28$). Overall, the average S^2 value for TTD bound to heparin is 0.69; the average S^2 value for TTD in the free state is 0.54.

DISCUSSION

Structure and Dynamics of TTD in the Free State. Our long-term goal is to characterize the mechanism of TTD-mediated translocation across biological membranes, which has been shown to be important in AIDS pathogenesis and promises to be an important biotechnological tool in the future. Toward this goal, we have prepared a model system, PG-TTD, for the study of the TTD mechanism. As demonstrated by NMR, the TTD moiety in the context of a cargo protein is in an extended conformation and relatively dynamic in the free state. This observation is consistent with CD studies of the TTD peptide in the free state (*31*, *32*, Caffrey, unpublished results). Moreover, a recent NMR structure of full-length tat shows the TTD to be in an extended conformation (*33*). Interestingly, the lack of regular secondary structure of TTD may be an inherent property for membrane translocation. For example, transit sequences of plant chloroplast proteins have been proposed to be purposely devoid of structure (*34*). This notion is supported by CD and NMR studies of plant transit peptides in the presence of mixed micelles (*35*). Importantly, the structure and dynamic properties of the PG moiety are not disturbed by the presence of TTD, suggesting that TTD does not inherently destabilize the structure of the cargo protein. Thus, the cargo protein can be taken to be in the native structure in the extracellular *and* intracellular free states (i.e., before and after membrane translocation).

Heparin Binding to PG-TTD. Heparin is a naturally occurring analogue of heparan sulfate, which can be used as a model of heparan sulfate found on cell surfaces (*29*). Previously, we have demonstrated that PG-TTD binds to a heparin affinity column with relatively high affinity, based on elution of PG-TTD at 1.6 M NaCl (*14*). The present work has used ITC to determine the K_d of heparin binding to PG-TTD, as well as the ΔH and ΔS of heparin binding. The measured K_d of the PG-TTD/heparin complex is 0.37 μM, which is similar to those observed for various FGF/heparin complexes, which range from 0.5 to 85 μM (*29*). Interestingly, the stoichiometry of heparin binding suggests that multiple PG-TTD bind to 1 heparin molecule. Multiple binding sites are reasonable in the case of heparin, which consists of multiple repeating disaccharide units. For example, the X-ray structure of the FGF/heparin complex shows that heparin binds multiple FGF (*36*, *37*). On the basis of the negative ΔH, the binding of TTD to heparin is driven

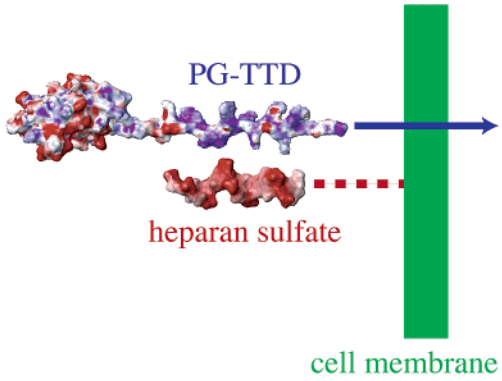

FIGURE 6: Model for the interaction between PG-TTD and heparan sulfate proteoglycans. The coordinates for the PG moiety of PG-TTD were taken from the solution structure of PG (*21*). The coordinates for TTD and the linker regions were modeled in an extended conformation using the program CNS 1.0 (*22*). The coordinates for heparin, an analogue of heparan sulfate, were taken from those of the X-ray structure of the ternary complex of heparin, FGF, and the FGF receptor (*37*). The electrostatic profile was calculated by the program MOLMOL (*24*).

by the formation of energetically favorable interactions between the basic side chains of TTD and the negative sulfate groups of heparin. Finally, the negative ΔS predicts that the entropy of PG-TTD and/or heparin is decreased in the complex. In general, the S^2 of PG-TTD increased upon binding to heparin, consistent with increased order and decreased entropy. Previous NMR studies of other proteins have demonstrated that changes in S^2 can be directly related to entropy (cf. *38*). However, the entropy changes relate to the global order of the complex, which is comprised of backbone and side chain atoms, as well as the atoms of heparin. In the present case, the order parameters are known for the majority of the NH vectors but are missing for all other atoms within the complex; thus, we feel that it is unwise to calculate entropy from S^2 values of the PG-TTD/heparin complex.

Model of the PG-TTD/Heparin Complex. Work presented here and elsewhere (*8*−*10*) have suggested that the first step of TTD-mediated entry consists of TTD binding to heparan sulfate present on cell surfaces. In Figure 6 we present a model of the interaction between PG-TTD and heparin, an analogue of heparan sulfate. The model of PG-TTD was obtained by adding the TTD to the C-terminus of PG (*21*) and performing a restrained molecular dynamics simulation (*23*). As discussed above the structure of the PG moiety is unperturbed by the presence of TTD or heparin; thus, the PG structure can be taken from the solution structure (*21*). Proteins and peptides are known to bind to heparin in various conformations. For example, heparin binds to α-helical regions of antithrombin and to loop regions of various FGF (reviewed in ref *29*). Indeed, a peptide corresponding to the consensus heparin binding sequence has been shown to undergo a transition from an extended structure to an α helix in the presence of heparin (*39*, *40*). However, in the present study structure of the TTD moiety has been modeled in an extended conformation, based on the secondary NMR chemical shifts, NOEs and CD of TTD in the presence of heparin (presented above). The heparin structure shown consists of 10 monosaccharide units, which corresponds to ~half that of the heparin used in the present study. On the basis of the ITC results, an electrostatic interaction between positively charged TTD and negatively charged heparin is highlighted by their respective electrostatic potentials. It is important to note that the structure of heparin bound to PG-TTD may be in a different conformation. For example, the iduronate ring of heparin has been shown to be in equilibrium with two conformations (*37*, *41*). Regardless of the heparin conformation, it is clear that heparin presents a negatively charged surface to interact with the positively charged surface of the TTD moiety. Importantly, heparin is an analogue of heparan sulfate found at the cell surface of many cell types. Thus, the interaction between the TTD and solubilized heparin may indeed mimic the physiological interaction with heparan sulfate, with the caveat that the in vivo interaction between TTD and heparan sulfate may be modulated by variations of the carbohydrate sequence and/or the degree of sulfation. Finally, it is important to note that TTD binding to cell surface receptors may also be involved in TTD-mediated entry. For example, tat binding to the low-density lipoprotein receptor-related protein of neuronal cells, as well as heparan sulfate proteoglycans, has also been shown to be critical to tat entry (*42*).

ACKNOWLEDGMENT

The work of Nikolina Sekulic in preliminary studies of PG-TTD is gratefully acknowledged.

SUPPORTING INFORMATION AVAILABLE

Two tables S1 and S2, which contain the relaxation data (R_z, R_{xy}, and HNOE) and the derived relaxation parameters (S^2, τ_e, R_{ex}, and $S_f{}^2$) for PG-TTD in the free and heparin-bound states. This material is available free of charge via the Internet at http://pubs.acs.org.

REFERENCES

1. Vives, E., Brodin, P., and Lebleu, B. (1997) A truncated HIV-tat protein basic domain rapidly translocates through the plasma membrane and accumulates in the cell nucleus. *J. Biol. Chem. 272*, 16010−16017.
2. Futaki, S. (2002) Arginine-rich peptides: potential for intracellular delivery of macromolecules and the mystery of the translocation mechanisms. *Int. J. Pharm. 245*, 1−7.
3. Westendorp, M., Frank, R., Ochsenbauer, C., Stricker, K., Dhein, J., Walczak, H., Debatin, K., and Krammer, P. (1995) Sensitization of T-cells to CD95-mediated apoptosis by HIV-1 tat and gp120. *Nature 375*, 497−500.
4. Li, C., Friedman, D., Wang, C., Metelev, V., and Pardee, A. (1995) Induction of apoptosis in uninfected lymphocytes by HIV-1 tat protein. *Science 268*, 429−431.
5. Gallo, R. (1999) Tat as one key to HIV-induced immune pahtogenesis and Tat toxoid as an important component of a vaccine. *Proc. Natl. Acad. Sci. U.S.A. 96*, 8324−8326.
6. Schwarze, S., Ho, A., Vocero-Akbani, A., and Dowdy, S. (1999) In vivo protein transduction: delivery of a biologically active protein into the mouse. *Science 285*, 1569−1572.
7. Schwarze, S., and Dowdy, S. (2000) In vivo protein transduction: intracellular delivery of biologically active proteins, compounds and DNA. *Trends Pharm. Sci. 21*, 45−48.
8. Rusnati, M., Doltrini, D., Oreste, P., Zoppetti, G., Albini, A., Noonan, D., Fagagna, F., Giacca, M., and Presta, M. (1997) Interaction of HIV-1 tat protein with heparin. *J. Biol. Chem. 272*, 11313−11320.
9. Rusnati, M., Tulipano, G., Urbanti, C., Tanghetti, E., Giuliani, R., Giacca, M., Ciomei, M., Corallini, A., and Presta, M. (1998) The basic domain in HIV-1 tat protein as a target for polysulfonated heparin-mimicking extracellular tat antagonists. *J. Biol. Chem. 273*, 16027−16037.

10. Tyagi, M., Rusnati, M., Presta, M., and Giacca, M. (2001) Internalization of HIV-1 tat requires cell surface heparan sulfate proteoglycans. *J. Biol. Chem. 276*, 3254−3261.
11. Silhol, M., Tyagi, M., Giacca, M., Leblue, B., and Vives, E. (2002) Different mechanisms for cellular internalization of the HIV-1 tat-derived cell penetrating peptide and recombinant proteins fused to tat. *Eur. J. Biochem. 269*, 494−501.
12. Richard, J., Melikov, K., Vives, E., Ramos, C., Verbeure, B., Gait, M., Chernomordik, L. and Lebleu, B. (2003) Cell-penetrating peptides. A reevaluation of the mechanism of cellular uptake. *J. Biol. Chem. 278*, 585−590.
13. Takeshima, K., Chikushi, A., Lee, K.-K., Yonehara, S., and Matsuzaki, K. (2003) Transolocation of analogues of the antimicrobial peptides magainin and buforin across human cell membranes. *J. Biol. Chem. 278*, 1310−1315.
14. Hakansson, S., Jacobs, A., and Caffrey, M. (2001) Heparin Binding by the HIV-1 tat protein transduction domain. *Protein Sci. 10*, 2138−2139.
15. Huth, J., Bewley, C., Jackson, B., Hinnebusch, A., Clore, G., and Gronenborn, A. (1997) Design of an expression system for detecting folded protein domains and mapping macromolecular interactions by NMR. *Protein Sci. 6*, 2359−2364.
16. Marley, J., Lu, M., and Bracken, C. (2001) A method for efficient isotopic labeling of recombinant proteins. *J. Biomol. NMR 20*, 71−75.
17. Blumenkrantz, N., and Asboe-Hansen, G. (1973) New method for quantitative determination of uronic acids. *Anal. Biochem. 54*, 484−489.
18. Cavanagh, J., Fairbrother, W., Palmer, A., and Skelton, N. (1996) in *Protein NMR Spectroscopy*, Academic Press, San Diego.
19. Delaglio, F., Grzesiek, S., Vuister, G., Zhu, G., Pfeifer, J., and Bax, A. (1995) NMRPipe: a multidimensional spectral processing system based on UNIX pipes. *J. Biomol. NMR 6*, 277−293.
20. Dosset, P., Hus, J., Blackledge, M., and Marion, D. (2000) Efficient analysis of macromolecular rotational diffusion from heteronuclear relaxation data. *J. Biomol. NMR 16*, 23−28.
21. Gronenborn, Filpula, D., Essig, N., Achari, A., Whitlow, M., Wingfield, P., and Clore, G. (1991) A novel, highly stable fold of the immunoglobulin binding domain of streptococcal protein G. *Science 253*, 657−661.
22. Lipari, G., and Szabo, A. (1982) Model-free approach to the interpretation of nuclear magnetic resonance relaxation in macromolecules. 1. Theory and range of validity. *J. Am. Chem. Soc. 104*, 4546−4559.
23. Brunger, A., Adams, P., Clore, G., DeLano, W., Gros, P., Grosse-Kunstleve, R., Jiang, J.-S., Kuszewski, J., Nilges, M., Pannu, N., Read, R., Rice, L., Simonson, T., and Warren, G. (1998) Crystallography and NMR System: a new software suite for macromolecular structure determination. *Acta Crystallogr. D54*, 905−921.
24. Koradi, R., Billeter, M., and Wuthrich, K. (1996) MOLMOL: a program for display and analysis of macromolecular structures. *J. Mol. Graphics 14*, 52−55.
25. Barchi, J., Grasberger, B., Gronenborn, A., and Clore, G. (1994) Investigation of the backbone dynamics of the IgG-binding domain of streptococcal protein G by heteronuclear two-dimensional ^{1}H-^{15}N nuclear magnetic resonance spectroscopy. *Protein Sci. 3*, 15−21.
26. Wishart, D., and Case, D. (2001) Use of chemical shifts in macromolecular structure determination. *Methods Enzymol. 338*, 3−34.
27. Palmer, A. (1997) Probing molecular motions by NMR. *Curr. Opin. Struct. Biol. 7*, 732−737.
28. Kay, L. (1998) Protein dynamics from NMR. *Nat. Struct. Biol. 5*, 513−517.
29. Conrad, H. (1998) in *Heparin Binding Proteins*, Academic Press, San Diego, CA.
30. Shuker, S., Hajduk, P., Meadows, R., and Fesik, S. (1996) Discovering high-affinity ligands for proteins: SAR by NMR. *Science 274*, 1531−1534.
31. Loret, E., Vives, E., Ho, P., Rochat, H., Vanrietschoten, J., and Johnson, W. (1991) Activating region of HIV-1 tat protein: vacuum UV circular dichrosim and energy minimization. *Biochemistry 30*, 6013−6023.
32. Mabrouk, K., Vanrietschoten, J., Vives, E., Darbon, H., Rochat, H., and Sabatier, J. (1991) Lethal neurotoxicity in mice of the basic domains of HIV and SIV rev proteins. Study of these regions by circular dichrosim. *FEBS Lett. 289*, 13−17.
33. Gregoire, C., Pelopenese, J.-M., Esquieu, D., Opi, S., Campbell, G., Solomiac, M., Lebrun, E., Lebreton, J., and Loret, E. (2001) Homonuclear 1H NMR assignment and structural characterization of human immunodeficiency virus type 1 tat Mal protein. *Biopolymers 62*, 324−335.
34. Von Heijne, G., and Nishikawa, K. (1991) Chloroplast transit peptides-the perfect random coil. *FEBS Lett. 278*, 1−3.
35. Wienk, H., Wechselberger, R., Czisch, M., and de Kruijff, B. (2000) Structure, dynamics and insertion of a chloroplast targeting peptide in mixed micelles. *Biochemistry 39*, 8219−8227.
36. Pellegrini, L., Burke, D., Von Delft, F., Mulloy, B., and Blundell, T. (2000) Crystal structure of fibroblast growth factor receptor ectodomain bound to ligand and heparin. *Nature 407*, 1029−1034.
37. Faham, S., Hileman, R., Fromm, J., Linhardt, R., and Rees, D. (1996) Heparin structure and interactions with basic fibroblast growth factor. *Science 271*, 1116−1120.
38. Stivers, J., Abeygunawardana, C., Milvan, A., and Whitman, C. (1996) ^{15}N NMR relaxation studies of free and inhibitor-bound 4-oxalocrotonate tautomerase: backbone dynamics and entropy changes of an enzyme upon inhibitor binding. *Biochemistry 35*, 16036−16047.
39. Jayaraman, G. Wu, C., Liu, Y., Chien, K., Fang, J., and Lyu, P, (2000) Binding of a de novo designed peptide to specific glycosaminoglycans. *FEBS Lett. 482*, 154−158.
40. Verrecchio, A., Germann, M., Schick, B., Kung, B., Twardowski, T., and San Antonio, J. (2000) Design of peptides with high affinities for heparin and endothelial cell proteoglycans. *J. Biol. Chem. 275*, 7701−7707.
41. Mulloy, B., Forster, M., Jones, C., and Davies, D. (1993) NMR and molecular-modeling studies of the solution conformation of heparin. *Biochem. J. 293*, 849−858.
42. Liu, Y., Jones, M., Hingtgen, C., Bu, G., Laribee, N., Tanzi, R., Moir, R., Nath, A., and He, J. (2000) Uptake of HIV-1 tat protein mediated by low-density lipoprotein receptor-related protein disrupts the neuronal metabolic balance of the receptor ligands. *Nat. Med. 6*, 1380−1387.

BI020715+